Synthesis and size-dependent properties of zinc-blende semiconductor quantum rods

SHIHAI KAN, TALEB MOKARI, ELI ROTHENBERG AND URI BANIN*

Institute of Chemistry, Farkas Center for Light Induced Processes and the Center for Nanoscience and Nanotechnology, The Hebrew University of Jerusalem, Jerusalem 91904, Israel
*e-mail: banin@chem.ch.huji.ac.il

Published online 9 February 2003; doi:10.1038/nmat830

Dimensionality and size are two factors that govern the properties of semiconductor nanostructures[1,2]. In nanocrystals, dimensionality is manifested by the control of shape, which presents a key challenge for synthesis[3–5]. So far, the growth of rod-shaped nanocrystals using a surfactant-controlled growth mode, has been limited to semiconductors with wurtzite crystal structures, such as CdSe (ref. 3). Here, we report on a general method for the growth of soluble nanorods applied to semiconductors with the zinc-blende cubic lattice structure. InAs quantum rods with controlled lengths and diameters were synthesized using the solution–liquid–solid mechanism[6] with gold nanocrystals as catalysts[7]. This provides an unexpected link between two successful strategies for growing high-quality nanomaterials, the vapour–liquid–solid approach for growing nanowires[8–12], and the colloidal approach for synthesizing soluble nanocrystals[13–15]. The rods exhibit both length- and shape-dependent optical properties, manifested in a red-shift of the bandgap with increased length, and in the observation of polarized emission covering the near-infrared spectral range relevant for telecommunications devices[16,17].

The rod architecture exhibits potential technological advantages over spherical nanocrystals, as already demonstrated in the observation of linearly polarized emission and lasing from quantum rods (QRs) in the visible range[18,19], and in improved photocell performance[20]. The previously used surfactant-controlled rod-growth approach is based on the presence of chemically dissimilar lattice faces that can be selectively bound by coordinating ligands to achieve different growth rates along different crystal axes[3,21]. The approach presented here for rod growth is particularly needed for lattice structures that do not obviously present such chemically dissimilar surfaces, as is the case for materials with a zinc-blende cubic lattice. Our method uses the solution–liquid–solid (SLS) mechanism that can be considered as an extension of the vapour–liquid–solid (VLS) mechanism widely used for growth of crystalline wire-like structures[22], and more recently nanowires[8–12]. In both methods, a liquid metal cluster acts as a catalyst where reactants dissolve, subsequently leading to directed growth from the supersaturated drop. The first reported use of the SLS mechanism was in the growth of insoluble whiskers of III-V semiconductors at low temperature[6]. Micrometre long silicon nanowires with diameters of 4–5 nm were also prepared in a pressurized solution system by using gold nanocrystals as a catalyst[7]. In these reports, the control of length was not achieved. Length control is desirable from the viewpoint of the chemical processability of QRs that are soluble, unlike insoluble wires. In spherical nanocrystals, such chemical accessibility enabled the use of powerful self-assembly approaches to realize a wide range of applications such as biological fluorescence[23,24] and Raman-based[25] marking, photovoltaics[20], light-emitting diodes[16,26] and lasers[27]. Moreover, as we demonstrate here, controlling the length can provide further tuning for the optical and electronic properties with both basic and applied significance.

To obtain solution-processable QRs of III-V semiconductors with controlled lengths and diameters, we employ gold nanoparticles to catalyze and direct one-dimensional rod growth. For InAs QRs, we use the reaction between tris(trimethylsilyl)arsine ($(TMS)_3As$) and $InCl_3$ in trioctylphosphine oxide (TOPO), based on the successful procedure for growing high-quality spherically shaped InAs nanocrystals (see Supplementary Information, Fig. S1)[14]. Dodecanethiol-stabilized gold nanoparticles with diameter of ~2 nm were prepared using known methods[28], these particles being readily soluble in the stock solution of the rod synthesis. This allows for the injection of the gold nanoparticles together with the precursors, which was found to be critical for shape control of the InAs system.

In a typical experiment conducted under argon flow, a growth solution was heated to 360 °C. A stock solution containing the reagents and gold particles was then injected into the growth solution within 0.1 s under vigorous stirring, leading to the decrease of the reaction temperature to about 300 °C. Less then 3 s later, 2 g cold trioctylphosphine (TOP) was injected to further quench the temperature to ~220 °C, and the reaction was then cooled to room temperature. The process yielded InAs QRs with a uniform diameter but broad length distribution, along with by-products, including a small fraction of InAs quantum dots, InAs nanowires and gold particles. Optimization of the synthesis conditions was carried out in relation to the relative gold content and the volume ratio between the stock solution and the growth solution (see Supplementary Information).

The rods were purified and size-selected by centrifugation. QRs and nanowires were obtained in different fractions. Figure 1a–c presents transmission electron microscopy (TEM) images of three fractions of nanorods, all with mean diameters of 4 nm, and varying mean lengths

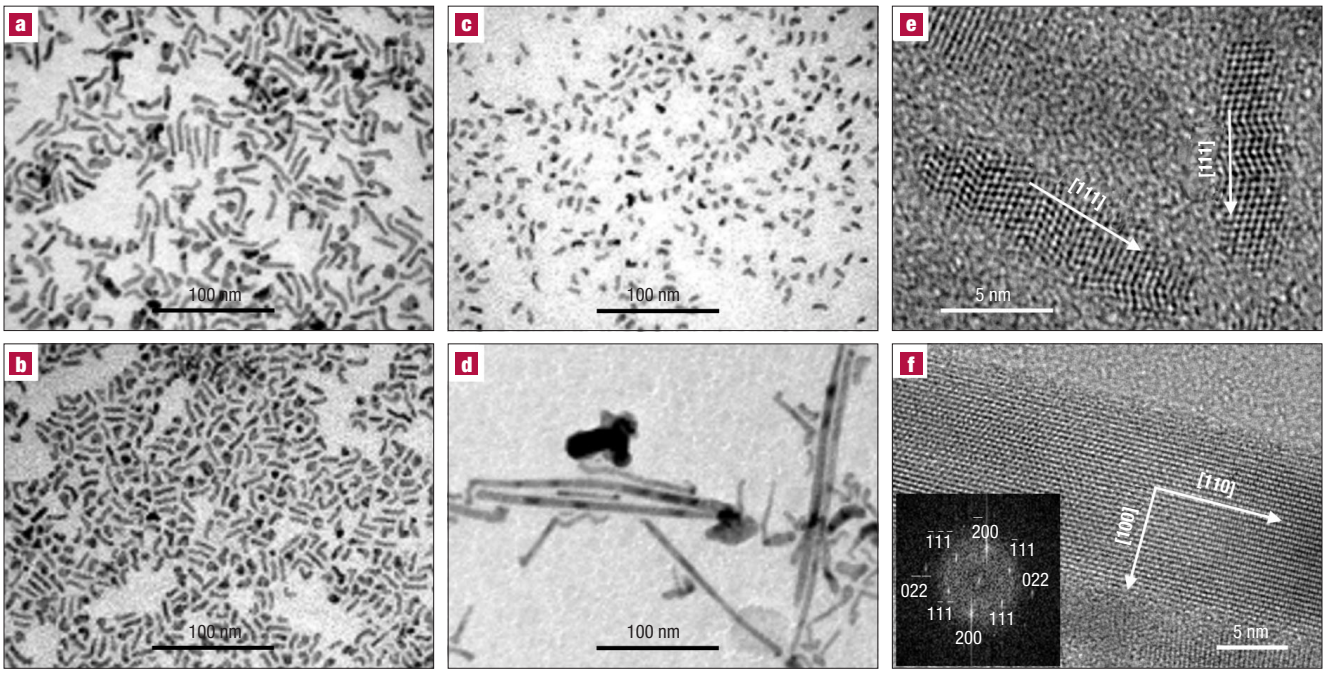

Figure 1 TEM images of the reaction products. a–c, The first to third fractions of InAs nanorods, respectively. The rods are seen to have different lengths but similar diameter. Some of the rods, in particular longer ones, are kinked. **d**, The fraction with nanowires up to 20 nm in diameter and lengths ranging from 0.1 to 1 μm. **e**, HRTEM image of InAs nanorods 12 × 4 nm. The measured distance between neighbouring planes along the growth axis is 3.5 Å, matching the *d* value for InAs [111] planes (3.48 Å). Stacking faults are seen, observed by the zig-zag pattern. **f**, HRTEM image of part of a nanowire with total dimensions 200 × 12 nm. The wire, without stacking faults, grows along the InAs [110] direction. Inset, Fourier transform of the image, indicating that the rod is viewed along the [111] zone axis of the cubic structure.

of 22.7 nm (Fig. 1a), 15.1 nm (Fig. 1b), and 9.4 nm (Fig. 1c). In Fig. 2, histograms representing the diameter and length distributions in these three nanorod fractions are shown, clearly revealing the similar diameters and varying lengths. The width of the diameter distribution is 15%, and the length distribution width is 20%. Gold particles, with increased contrast, could be identified at the end of many of the rods (see also Supplementary Information, Fig. S2). Figure 1d shows a TEM image of a fraction of nanowires obtained from the first separation stage. The method clearly provides length-controlled QRs, and was also applied to InP, demonstrating its generality (see Supplementary Information, Fig. S3). The as-prepared InAs nanorods were crystalline, as indicated in the powder X-ray diffraction (XRD) pattern (Fig. 3a), matching the bulk InAs peak structure, and in high-resolution TEM (HRTEM) images of individual rods (Fig. 1e). The planes perpendicular to the rod axis are evenly separated by ~3.5 Å, matching the [111] *d*-spacing of InAs. Stacking faults are observed, which are probably due to the low growth temperature and short reaction time, which may also explain the kinking in some of the longer rods.

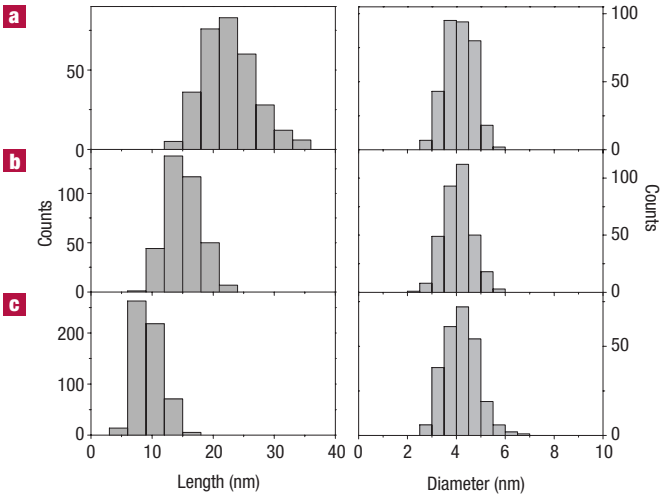

Figure 2 Size-distribution histograms for InAs quantum rods. The distributions of both length and diameters, extracted from the TEM images for more then 300 particles for each sample, are shown in frames **a–c**, corresponding to the three fractions of nanorods shown in Fig. 1a–c, respectively. Mean sizes and size distributions for length, diameter, are: **a**, 22.7 ± 4.4 nm, 4.0 ± 0.6 nm. **b**, 15.1 ± 2.7 nm, 4.1 ± 0.7 nm. **c**, 9.4 ± 2.1 nm, 4.1 ± 0.6 nm.

Figure 3b shows the XRD pattern of the nanowires from Fig. 1d. The InAs peaks are significantly narrower than those observed for the rods, due to the larger crystalline domain size. Additionally, the [220] and [311] peaks of InAs are stronger than the [111] peak, unlike the rods, indicating that the growth of the nanowires takes place along the [110] or the [311] direction. This is further supported by the HRTEM image of the wires (Fig. 1f and Supplementary Information, Fig. S4).

The SLS and VLS mechanisms suggest that a liquefied metallic particle acting as a catalyst is needed for one-dimensional growth[6,8]. The reaction temperature in our method is surprisingly low (~700 degrees below the melting point of bulk gold). This is possible because of the well-documented phenomena of a decrease in the melting temperature of nanocrystals with reduced size[29]. Syntheses at a lower reaction temperature of 300 °C, did not yield one-dimensional growth, indicating that the conditions are at the onset of melting. This is consistent with theoretical studies indicating that the melting temperature for Au_{146} (diameter ~1.6 nm) was ~350 °C, increasing to ~480 °C in Au_{459} clusters (diameter ~2.5 nm), and before melting, there

is a region of temperature where increased atomic diffusion near the surface takes place in the smaller clusters[30,31]. This may suffice for achieving the required function of the gold particles as catalysts. Notably, this temperature is below the boiling point of TOPO, a coordinating solvent for synthesis of high-quality nanocrystals[13,14], allowing for the implementation of this method to achieve rod growth. This allows a remarkable link to be obtained between the method of growing nanowires in the gas-phase by the VLS mechanism, and the colloidal approach of synthesizing soluble nanocrystals through the pyrolysis of suitable precursors in coordinating solvents.

The importance of length and shape control for modifying the optical properties of the QRs is demonstrated in Fig. 4a, presenting the optical absorption and photoluminescence (PL) spectra of InAs rods of different lengths, along with InAs dots with a diameter similar to that of the rods. A gradual red-shift of the bandgap appears from dots to short rods and to longer rods, indicating strong quantum confinement in the length direction, to the extent that the PL of QRs can effectively cover the telecommunications bands at 1.2–1.5 μm. The shift of the bandgap with length is shown in Fig. 4b, along with a simulation of this effect using a cylindrical particle-in-a-box model. The present case of InAs QRs differs from the case of CdSe QRs, where minimal length-dependent effects could be discerned in the optical spectra of rods longer than ~10 nm[32,33]. The bulk exciton Bohr radius, 5 nm in CdSe, compared with 35 nm in InAs, provides an effective ruler for qualitative understanding of this difference between the two materials. Whereas in the CdSe rods, the length is governed by medium to weak confinement, in InAs rods the length is still in a strongly quantum-confined regime.

The observed bandgap red-shift with length in InAs rods is accompanied by a significant reduction in the PL intensity (Fig. 4c). This is also a signature of the gradual evolution of the confinement

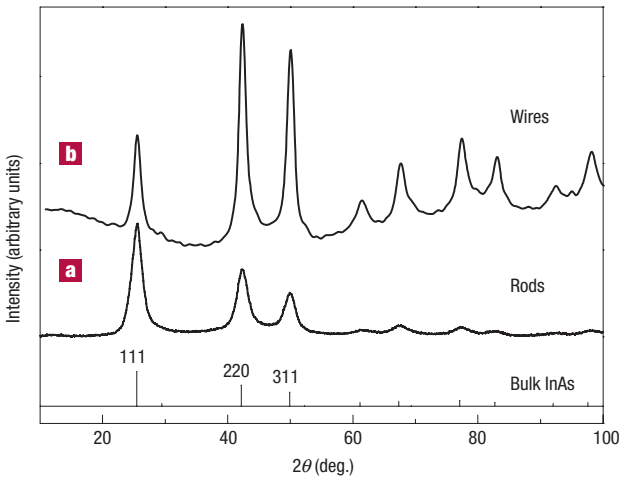

Figure 3 Powder X-ray diffraction patterns of the reaction products. a, InAs nanorods with mean dimensions 22.7 × 4.0 nm as shown in Fig. 1a. **b**, Nanowires shown in Fig. 1d. The lines represent the diffraction peaks of bulk InAs.

in the long rod axis. Owing to the significant difference in the electron and hole effective masses ($0.024m_o$ and $0.4m_o$ for the electron and hole, respectively, where m_o is the free electron mass), the electron wavefunction is still delocalized over the entire rod (strong confinement), whereas the hole is in a medium confinement regime, and the extent of

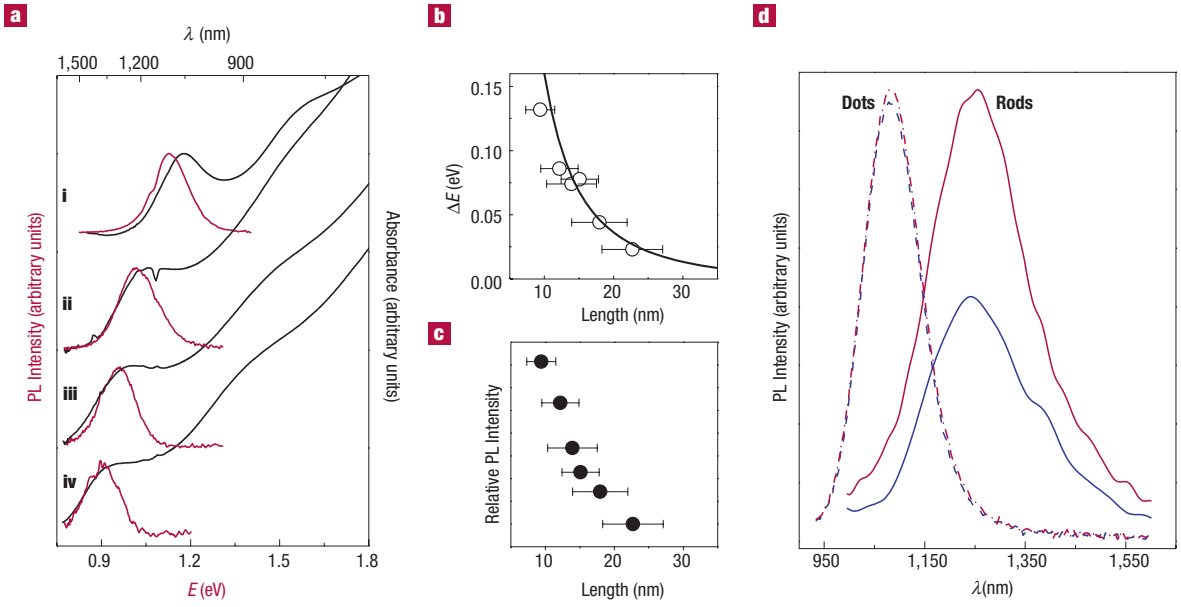

Figure 4 Length-dependent optical properties of InAs semiconductor quantum rods. a, Room-temperature absorption (black lines) and photoluminescence (red lines) spectra in toluene solution of (i) InAs quantum dots, 4 nm in diameter; (ii) quantum rods 9.4 × 4.1 nm (mean length by diameter) as shown in Fig. 1c; (iii) quantum rods, 15.1 × 4.1 nm, as shown in Fig. 1b; (iv) quantum rods, 22.7 × 4.0 nm, as shown in Fig. 1a. The PL intensity was normalized for clarity of presentation. **b**, Shift of the bandgap of InAs quantum rods (taken as the peak of the PL) as a function of rod length. Open circles, experimental results; solid line, model calculation results. The model assumes an infinite barrier cylindrical box with diameter of 4 nm, using the bulk InAs effective masses. The shift was calculated relative to the bandgap of the infinitely long wire. The experimental data were offset accordingly, by 0.88 eV, as part of the fitting process. **c**, Dependence of the PL intensity on rod length showing decreased PL in longer rods. The error bars signify the width of the length distribution for the samples. **d**, Polarized emission measurements of InAs quantum rods and quantum dots. Solid lines are PL in InAs rods, and dashed lines are PL of the dots, both in stretched polymer (polyvinyl-butyral) films. The excitation polarization was set parallel to the stretch axis, and the PL was measured either parallel (red) or perpendicular (blue) to this axis. Rods show a clear polarization dependence, unlike the dots.

its wavefunction is more limited[34]. Therefore, the overlap between electron and hole wavefunctions becomes smaller on increasing rod length, leading to a reduced radiative rate, and as a result, decreased luminescence efficiency.

An additional distinct signature of the change in optical properties with the symmetry is demonstrated in Fig. 4d, showing polarized PL measurements on 17×4 nm InAs rods and 4 nm dots, both in a stretched polymer film. The dots exhibit unpolarized PL corresponding to their spherical symmetry, whereas the rods show PL preferentially polarized along the stretching direction of the polymer, in accordance with their symmetry axis. This will enable the development of future QR-based optoelectronic devices in the telecommunications range, with desirable features such as polarized lasing or polarization-sensitive optical detectors[16,17]. These characteristics clearly demonstrate that such InAs quantum rods present possibilities for conducting new fundamental studies, as well as for new applications. The approach can also be used to grow InP nanorods, with potential importance in photovoltaic applications. Further expansion of the present method to grow soluble nanorods of additional materials, using a variety of possible metal nanoparticles as catalysts, may also be considered.

METHODS

InAs ROD SYNTHESIS

In a typical preparation, a four-necked flask was used, containing 2 g TOPO as the growth solution. The stock solution contained 100 mg (0.34 mmol) $(TMS)_3As$, 0.57 g (0.68 mmol) $InCl_3$/TOP solution (0.3 g ml^{-1}), and 0.5 g gold/toluene solution (6.7 mg g^{-1}) in 1 g TOP. The raw product was diluted with toluene and centrifuged in 5 ml vials at 6,000 r.p.m. (relative centrifugal force (r.c.f.) ~4,000*g*) for 20 min. In this first step, nanowires were precipitated together with other big particles while the nanorods and dots remained soluble. In the second step, nanorods were obtained. The particles were partially precipitated by adding methyl alcohol and then centrifuged at 6,000 r.p.m. (r.c.f. ~4,000*g*) for 10 min. The resulting precipitate was redissolved with toluene, and a fraction of nanorods with a mean length of 22.7 nm and diameter of 4.0 nm was obtained. This procedure was repeated providing a second and third fraction of InAs QRs with mean lengths of 15.1 nm and 9.4 nm, respectively. Following this, a diluted solution containing mostly InAs dots was left. The precipitate from the first step was re-dispersed by ultrasonication in toluene with TOPO added to stabilize the solution. The solution was then centrifuged at 4,000 r.p.m. (r.c.f. ~1,800g) for 20 min, and the supernatant mostly contained InAs nanowires with length ranging from 100 nm to 1 μm and diameters up to 20 nm.

$(TMS)_3As$ was synthesized locally. All other materials were purchased from Aldrich. TOP and TOPO were both purified by vacuum distillation. All other materials were used without further purification.

STRUCTURAL CHARACTERIZATION

Powder X-ray diffraction measurements were performed on a Philips PW1830/40 X-ray diffractometer operated at 40 kV and 30 mA with CuK_α radiation. Samples were washed with methanol and deposited as a thin layer on a low-background-scattering quartz substrate. TEM measurements were performed on a Philips CM 120 microscope operated at 100 kV. HRTEM measurements were performed on a JEOL-JEM 2010 electron microscope operated at 200 kV. Samples for TEM were prepared by depositing a drop of sample toluene solution onto 400 mesh copper grids covered with a thin amorphous carbon film, followed by washing with methanol to remove the excess organic residue.

OPTICAL CHARACTERIZATION

Absorption spectra were measured using a Shimadzu 1601 spectrophotometer for the region up to 1.1 μm, and above this wavelength with a home-built set-up using a monochromatized tungsten lamp with a Ge detector and lock-in amplification. PL spectra were measured using a 635 nm diode laser for excitation. The emission was collected at a right-angle configuration, dispersed by a monochromator and detected by an InGaAs PIN photodetector with lock-in amplification.

Received 14 October 2002; accepted 6 January 2003; published 9 February 2003.

References

1. Alivisatos, A. P. Semiconductor clusters, nanocrystals, and quantum dots. *Science* **271,** 933–937 (1996).
2. Banin, U., Cao, Y. W., Katz, D. & Millo, O. Identification of atomic-like electronic states in indium arsenide nanocrystal quantum dots. *Nature* **400,** 542–544 (1999).
3. Peng, X. G. *et al.* Shape control of CdSe nanocrystals. *Nature* **404,** 59–61 (2000).
4. Tang, Z. Y., Kotov, N. A. & Giersig, M. Spontaneous organization of single CdTe nanoparticles into luminescent nanowires. *Science* **297,** 237–240 (2002).
5. Pacholski, C., Kornowski, A. & Weller, H. Self-assembly of ZnO: From nanodots to nanorods. *Angew. Chem. Int. Edn* **41,** 1188–1191 (2002).
6. Trentler, T. J. *et al.* Solution-liquid-solid growth of crystalline III-V semiconductors: An analogy to vapor-solid-liquid growth. *Science* **270,** 1791–1794 (1995).
7. Holmes, J. D., Johnston, K. P., Doty, R. C. & Korgel, B. A. Control of thickness and orientation of solution-grown silicon nanowires. *Science* **287,** 1471–1473 (2000).
8. Morales, A. M. & Lieber, C. M. A laser ablation method for the synthesis of crystalline semiconductor nanowires. *Science* **279,** 208–211 (1998).
9. Duan, X. F. & Lieber, C. M. General synthesis of compound semiconductor nanowires. *Adv. Mater.* **12,** 298–302 (2000).
10. Gudiksen, M. S., Wang, J. F. & Lieiber, C. M. Synthetic control of the diameter and length of single crystal semiconductor nanowires. *J. Phys. Chem. B* **105,** 4062–4064 (2001).
11. Huang, M. H. *et al.* Room-temperature ultraviolet nanowire nanolasers. *Science* **292,** 1897–1899 (2001).
12. Johnson, J. C. *et al.* Single gallium nitride nanowire lasers. *Nature Mater.* **1,** 106–110 (2002).
13. Murray, C. B., Norris, D. J. & Bawendi, M. G. Synthesis and characterization of nearly monodisperse CdE (E = S, Se, Te) semiconductor nanocrystallites. *J. Am. Chem. Soc.* **115,** 8706–8715 (1993).
14. Guzelian, A. A., Banin, U., Kadavanich, A. V., Peng, X. & Alivisatos, A. P. Colloidal chemical synthesis and characterization of InAs nanocrystal quantum dots. *Appl. Phys. Lett.* 69, 1432–1434 (1996).
15. Murray, C. B. *et al.* Colloidal synthesis of nanocrystals and nanocrystal superlattices. *IBM J. Res. Dev.* **45,** 47–55 (2001).
16. Tessler, N., Medvedev, V., Kazes, M., Kan, S. H. & Banin, U. Efficient near-infrared polymer nanocrystal light-emitting diodes. *Science* **295,** 1506–1508 (2002).
17. Wang, J. F., Gudiksen, M. S., Duan, X. F., Cui, Y. & Lieber, C. M. Highly polarized photoluminescence and photodetection from single indium phosphide nanowires. *Science* **293,** 1455–1457 (2001).
18. Hu, J. T. *et al.* Linearly polarized emission from colloidal semiconductor quantum rods. *Science* **292,** 2060–2063 (2001).
19. Kazes, M., Lewis, D. Y., Ebenstein, Y., Mokari, T. & Banin, U. Lasing from semiconductor quantum rods in a cylindrical microcavity. *Adv. Mater.* **14,** 317–321 (2002).
20. Huynh, W. U., Dittmer, J. J. & Alivisatos, A. P. Hybrid nanorod-polymer solar cells. *Science* **295,** 2425–2427 (2002).
21. Puntes, V. F., Krishnan, K. M. & Alivisatos, A. P. Colloidal nanocrystal shape and size control: The case of cobalt. *Science* **291,** 2115–2117 (2001).
22. Wagner, R. S. in *Whisker Technology* (ed. Levitt, A. P.) 47–119 (Wiley-Interscience, New York, 1970).
23. Bruchez, M., Moronne, M., Gin, P., Weiss, S. & Alivisatos, A. P. Semiconductor nanocrystals as fluorescent biological labels. *Science* **281,** 2013–2016 (1998).
24. Chan, W. C. W. & Nie, S. Quantum dot bioconjugates for ultrasensitive nonisotopic detection. *Science* **281,** 2016–2018 (1998).
25. Cao, Y. W. C., Jin, R. C. & Mirkin, C. A. Nanoparticles with Raman spectroscopic fingerprints for DNA and RNA detection. *Science* **297,** 1536–1540 (2002).
26. Colvin, V. L., Schlamp, M. C. & Alivisatos, A. P. Light-emitting diodes made from cadmium selenide. *Nature* **370,** 354–357 (1994).
27. Klimov, V. I. *et al.* Optical gain and stimulated emission in nanocrystal quantum dots. *Science* **290,** 314–317 (2000).
28. Brust, M., Walker, M., Bethell, D., Schiffrin, D. J. & Whyman, R. Synthesis of thiol-derivatised gold nanoparticles in a two-phase liquid-liquid system. *J. Chem. Soc. Chem. Commun.* 801 (1994).
29. Dick, K., Dhanasekaran, T., Zhang, Z. & Meisel, D. Size-dependent melting of silica-encapsulated gold nanoparticles. *J. Am. Chem. Soc.* **124,** 2312–2317 (2002).
30. Cleveland, C. L., Luedtke, W. D. & Landman, U. Melting of gold clusters: Icosahedral precursers. *Phys. Rev. Lett.* **81,** 2036–2039 (1998).
31. Cleveland, C. L., Luedtke, W. D. & Landman, U. Melting of gold clusters. *Phys. Rev. B* **60,** 5065–5077 (1999).
32. Katz, D. *et al.* Size-dependent tunneling and optical spectroscopy of CdSe quantum rods. *Phys. Rev. Lett.* **89,** 086801 (2002).
33. Li, L. S., Hu, J. T., Yang, W. D. & Alivisatos, A. P. Bandgap variation of size- and shape-controlled colloidal CdSe quantum rods. *Nano Lett.* **1,** 349–351 (2001).
34. Efros, Al. L. & Rosen, M. The electronic structure of semiconductor nanocrystals. *Annu. Rev. Mater. Sci.* **30,** 465–521 (2000).

Acknowledgements

Supported in part by the Deutsche–Israel Program, the Israel Science Foundation and the US–Israel Binational Science Foundation. We are grateful to Vladimir Ezersky for assistance in the HRTEM measurements.

Correspondence and requests for materials should be addressed to U.B.

Supplementary Information is available on the *Nature Materials* website (http://www.nature.com/naturematerials).

Competing financial interests

The authors declare that they have no competing financial interests.

15. Yang, P., Zhao, D., Margolese, D. I., Chmelka, B. F. & Stucky, G. D. Generalized syntheses of large-pore mesoporous metal oxides with semicrystalline frameworks. *Nature* **396,** 152–155 (1998).
16. Lee, B., Lu, D., Kondo, J. N. & Domen, K. Three-dimensionally ordered mesoporous niobium oxide. *J. Am. Chem. Soc.* **124,** 11256–11257 (2002).
17. Hwang, Y. K., Lee, K.-C. & Kwon, Y.-U. Nanoparticle route to mesoporous titania thin films. *Chem. Commun.* 1738–1739 (2001).
18. Yun, H. S., Miyazawa, K., Zhou, H. S., Honma, I. & Kuwabara, M. Synthesis of mesoporous thin TiO_2 films with hexagonal pore structure using triblock copolymer templates. *Adv. Mater.* **13,** 1377–1380 (2001).
19. Mcmillan, P. W. *Glass-Ceramics* (Academic, London, 1979).
20. Gaskell, P. H. Structure, glass formation and properties. *J. Non-Crystal. Solids* **192/193,** 9–22 (1995).
21. Lu, Y. *et al.* Self-assembly of mesoscopically ordered chromatic polydiacetylene/silica nanocomposites. *Nature* **410,** 913–917 (2001).
22. Inagaki, S., Guan, S., Ohsuna, T. & Terasaki, O. An ordered mesoporous organosilica hybrid material with a crystal-like wall structure. *Nature* **416,** 304–307 (2002).
23. Li, D., Kong, L., Zhang, L. & Yao, X. Sol-gel preparation and characterization of transparent $KTiOPO_4/SiO_2$ nanocomposite glass for second harmonic generation. *J. Non-Cryst. Solids* **271,** 45–55 (2000).
24. James, P. F., Iqbal, Y., Jais, U. S., Jordery, S. & Lee, W. E. Crystallisation of silicate and phosphate glasses. *J. Non-Cryst. Solids* **219,** 17–29 (1997).
25. Pinckney, L. R. & Beall, G. H. Nanocrystalline non-alkali glass-ceramics. *J. Non-Cryst. Solids* **219,** 219–227 (1997).
26. Fujishima, A. & Honda, K. Electrochemical photolysis of water at a semiconductor electrode. *Nature* **238,** 37–38 (1972).
27. O'Regan, B. & Gratzel, M. A low-cost, high-efficiency solar cell based on dye-sensitized colloidal TiO_2 film. *Nature* **353,** 737–739 (1991).
28. Bach, U. *et al.* Solid-state dye-sensitized mesoporous TiO_2 solar cells with high photon-to-electron conversion efficiencies. *Nature* **395,** 583–585 (1998).
29. Wagemaker, M., Kentgens, A. P. M. & Mulder, F. M. Equilibrium lithium transport between nanocrystalline phases in intercalated TiO_2 anatase. *Nature* **418,** 397–399 (2002).
30 Talavera, R. R., Vargas, S., Arroyo-Murillo, R., Montiel-Campos, R. & Haro-Poniatowski, E. Modification of the phase transition temperatures in titania doped with various cations. *J. Mater. Res.* **12,** 439–443 (1997).
31. Schmutz, C. *et al.* EXAFS, Raman and ^{31}P NMR study of amorphous titanium phosphates. *J. Non-Cryst. Solids* **170,** 250–262 (1994).

Acknowledgements

D.L. acknowledges the financial support of the Japanese Society of the Promotion of Science (JSPS) Fellowship for work carried out at the Energy Electronics Institute, AIST. H.Z. thanks M. Ichihara for help in TEM observations, and acknowledges partial research funding from JSPS, Japan Science and Technology Agency, AIST.
Correspondence and requests for materials should be addressed to H. Z.
Supplementary Information accompanies the paper on www.nature.com/naturematerials

Competing financial interests

The authors declare that they have no competing financial interests.

CORRIGENDUM

Synthesis and size-dependent properties of zinc-blende semiconductor quantum rods

SHIHAI KAN, TALEB MOKARI, ELI ROTHENBERG AND URI BANIN

Nature Materials **2**, 155–158 (2003).

In this letter, Fig. 1f and Supplementary Information Fig. S4 were partially wrongly characterized in relation to indexing the growth direction of InAs wires that are found in the precipitate. Both figures are corrected below. We additionally comment that we observed in the powder X-ray diffraction pattern of the precipitate containing InAs wires that the [220] and [311] peaks of InAs are stronger than the [111] peak, unlike the rods (Fig. 3 in the original paper). The strong relative intensity of the [220] peak indicates that the growth of the wires takes place along the <110> direction. This is further supported by the HRTEM image of the wires (Fig. 1f and Supplementary information, Fig. S4). The higher intensity of the [311] peak might be caused by other, non-wire shaped, crystalline InAs structures in this fraction.

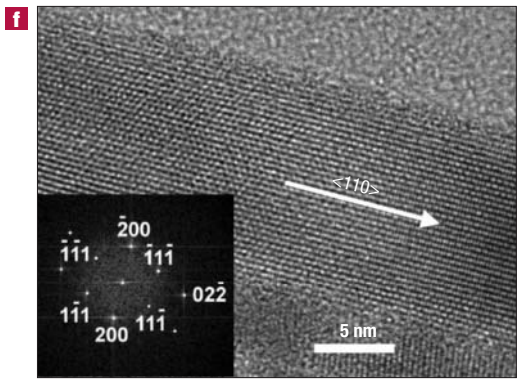

Figure 1f HRTEM image of part of a nanowire with total dimensions 200 × 12 nm. The wire, without stacking faults, grows along the InAs <110> direction. Inset: Fourier transform of the image, indicating that the wire is viewed along the <011> zone axis of the cubic structure.

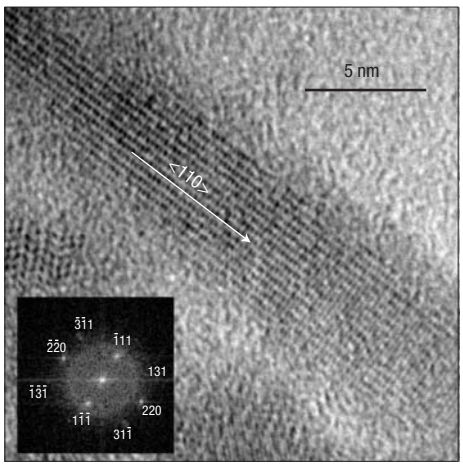

Figure S4 HRTEM of an InAs nanowire, ~200 × 5 nm in size. The wire grows along the [110] direction, as also indicated in the Fourier transform of the image viewed along the <112> zone axis.